HOSTED BY
ELSEVIER
CrossMark
Available online at www.sciencedirect.com
ScienceDirect
Progress in Natural Science: Materials International 24 (2014) 397–404
Progress in Natural Science Materials International
www.elsevier.com/locate/pnsmi
www.sciencedirect.com

Original Research

The ultrasonic modification of thermodynamic and kinetic regularity of lithium intercalation in talc ☆

O.V. Balaban[a,*], I.I. Grygorchak[a], R.M. Peleshchak[b], O.V. Kuzyk[b], O.O. Dan'kiv[b]

[a]*Lviv Polytechnic National University, Kotlyarevsky Street 1, Lviv 79013, Ukraine*
[b]*Drohobych Ivan Franko State Pedagogical University, Ivan Franko Street 24, Drohobych 82100, Ukraine*

Received 30 August 2013; accepted 20 May 2014
Available online 14 August 2014

Abstract

Influence of the ultrasound on talc ($Mg_3Si_4O_{10}(OH)_2$) cathode material was experimentally investigated. The Gibbs' energy change of the Li^+-intercalation process, the diffusion coefficient in $Li_xMg_3Si_4O_{10}(OH)_2$, the charge transfer resistance and the capacitance of the electric double layer were studied in electrochemical cells, based on initial and ultrasonic treated talc. The obtained results were interpreted within the nonlinear diffusion-deformation model, which involved formation of vacancy nanoclusters under ultrasonic influence at temperatures lower than a critical value.
© 2014 Chinese Materials Research Society. Production and hosting by Elsevier B.V. All rights reserved.

Keywords: Talc; Lithium intercalation; Gibbs' energy; Diffusion coefficient; Deformation; Vacancy

1. Introduction

Intercalation is the reversible insertion of molecule (or ion) into guest position of compounds with layered structures. Furthermore, intercalation provides a significant increase in specific energy of power sources, because strongly correlated bertollide phases are formed as a result of current generation process. The technical implementation of such process causes the appearance of lithium and lithium-ion batteries at the market. Today searching of new cathode materials for these applications is almost the most important task of material science. Taking into account the urgent problems of high prices of one Wh, ecological compatibility and resource base formation for use in the foreseeable future, it is obvious to focus on natural minerals. For this purpose they should have a system of the guest positions and provide good lithium diffusion and energy of lithium insertion, chemical and electrochemical stability, appropriate structure of the energy spectrum [1] conjugated with voltage range. We have proved that talc could be this mineral [2]. However, generally, the combination of all above listed characteristics in a certain mineral is implemented rarely. Therefore target modification of talc takes a lead place in improving efficiency of intercalation reaction. It was shown [3] that doping of talc powders could change its band structure in desired direction and as a result could improve both the energy and the power characteristics of lithium power sources. In this paper, we proposed ultrasonic treatment [4–6], as a new method of modification, which belongs to one of the most effective, cheap and environmentally safe technologies.

2. Experimental

Monodispersed talc powders with average grain size of 1 and 0.5 μm were used in experiments. Ultrasonic treatment of each talc fractions (0.2 g) was carried out in 2 ml of 1 M $LiBF_4$ in γ-butyrolactone solution during 8 h at the frequency of 22 kHz.

Electrodes of 0.25 cm^2 area on a nickel substrate were formed for research. The cathode mixture consisted of active

*Corresponding author. +380 684348103.
E-mail address: ksjsha502@gmail.com (O.V. Balaban).
Peer review under responsibility of Chinese Materials Research Society.

http://dx.doi.org/10.1016/j.pnsc.2014.07.003
1002-0071/© 2014 Chinese Materials Research Society. Production and hosting by Elsevier B.V. All rights reserved.

material (talc), conductive additive (acetylene soot), binding agent in the ratio 85:10:5 wt%. Mass of active material did not exceed 2.5 mg/electrode. Thermodynamic and kinetic parameters of lithium intercalation were investigated in three-electrode electrochemical cell in 1 M $LiBF_4$ in γ-butyrolactone solution and a chlorine-silver reference electrode. Nyquist diagrams were investigated in the frequency range from 10^{-3} to 10^{6} Hz using impedance spectrometer "AUTOLAB" ("ECO CHEMIE", Netherlands), equipped with computer applications FRA-2 and GPES. Computer modeling of the obtained impedance data was carried out in the software package ZView 2.3 (Scribner Associates). X-ray diffraction (XRD) measurements were performed on a DRON-3 under Co-Kα-radiation.

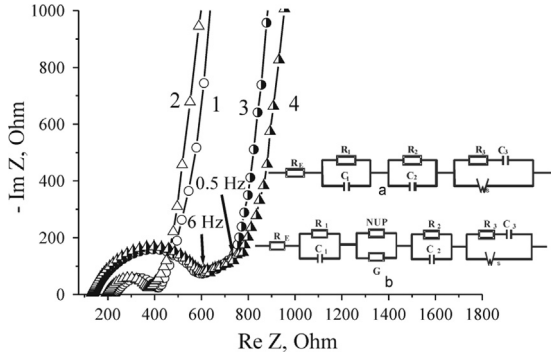

Fig. 2. Nyquist diagrams of 1 μm (1, 3) and 0.5 μm talc fractions (2, 4), before (1, 2) and after (3, 4) ultrasonic modification. The insets are equivalent electric circuits.

3. Results and discussion

Dependence of Gibbs' energy change ($\Delta G(x)$) of Li^+-intercalation process in talc fractions before and after ultrasonic treatment vs. the guest load degree x (x is a number of inserted guest atoms per one structural unit of host material) is shown in Fig. 1. First of all, one should pay attention to the behavior of curves 1 and 2 in Fig. 1. Since reduction of initial talc powders size from 1 μm to 0.5 μm leads to disappearance of the Ist order phase transition in x range from 0 to 2.5 and formation of strongly correlated single-phase states. The 1 μm talc fraction has higher energy storage in the high lithiated phases ($x > 4.5$). After ultrasonic treatment of talc fractions the phase diagram of their intercalated phase has changed completely. The range of two-phase states of the 1 μm fraction is divided into three intervals: with higher ($0 < x < 0.8$), lower ($0.8 < x < 1.5$) and ($1.5 < x < 4.5$) energy storage. The range of two-phase states of the 0.5 μm fraction changes both width ($0.8 < x < 3$) and values of ΔG ($3 < x < 5$).

Kinetics of Li^+-intercalation processes in $Li_xMg_3Si_4O_{10}(OH)_2$ at room temperature both before and after ultrasonic treatment (Fig. 2) cannot be described by the Rendls–Ershler classical model [7] because the slope angle of the low frequency branches of Nyquist plots to Re Z axis of the complex impedance differes from 45°. The most probable

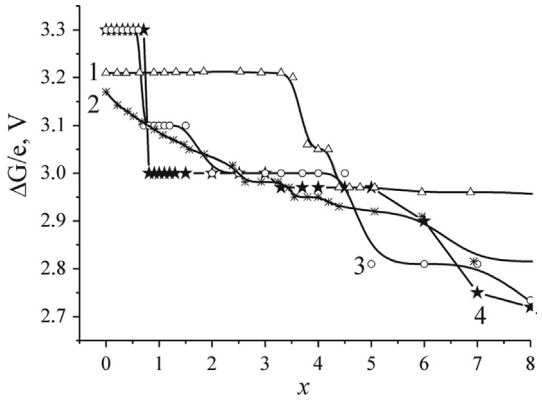

Fig. 1. Gibbs' energy change of lithium intercalation process in talc $Mg_3Si_4O_{10}(OH)$ powder of fractions: 1 μm (1, 3) and 0.5 μm (2, 4), before (1, 2) and after (3, 4) ultrasonic treatment.

reason for this is that the lithium diffusion in the volume of talc particles is not described by the ideal Fick's law. This in turn provides application of finite Warburg impedance [7] as a structural diffusion element in the impedance model. In the proposed equivalent electrical scheme (inset a, Fig. 2) R_E is resistance of an electrolyte, the series of parallel units of $R_1\|C_1$ and $R_2\|C_2$ consecutively attached to the Rendls–Ershler modified chain $W_s\|(R_3\text{-}C_3)$ simulates charge transfer through the barriers between grains (and possibly passivation film) and through the space charge region in the talc particle, respectively.

Computer modeling of the obtained impedance data in the software package ZView 2.3 determines the kinetic parameters of the intercalation process for all values of x. Verification of adequacy of the constructed model to the experimental data shows that Kramers–Kroning's coefficient does not exceed 3×10^{-5}.

Nyquist plots indicate the diffusion-kinetic control of the intercalation process. It means that limiting parameters of power capability are the lithium diffusion $D(x)$ in talc and the charge transfer resistance $R_3(x)$ through the interface of talc and electrolyte. As it is shown in Fig. 3 the kinetic parameters essentially depend on the conditions of ultrasonic effect on talc. At the same time ultrasonic treatment significantly increases power capacity even at sufficiently deep discharge levels ($x \approx 4$). It is interesting to note that the Ist order phase transitions (Fig. 1) are observed in the vicinity of this value of x. Extraordinary is the fact that both $D(x)$ and $R_3(x)$ oscillate with concentration only after ultrasonic modification (insets, Fig. 3). Hypothetically, such behavior can be explained by changes in electronic energy topology caused by ultrasonic effect on defective subsystem.

The XRD analysis of both samples before and after intercalation confirms impact of ultrasound on defect subsystem. First of all, aftereffect of ultrasonic treatment on the talc structure depends on the particle size. Ultrasonic treatment of the 1 μm fraction greatly reduces the width of the main peaks at $2\Theta = 11.00$ and 33.39°. Moreover treatment reformats the intense doublet at $2\Theta = 22.05$ and 22.59° into one peak at $2\Theta = 22.17°$. Ultrasonic treatment of the 0.5 μm fraction reduces intensity of the indicated diffraction peaks and slightly

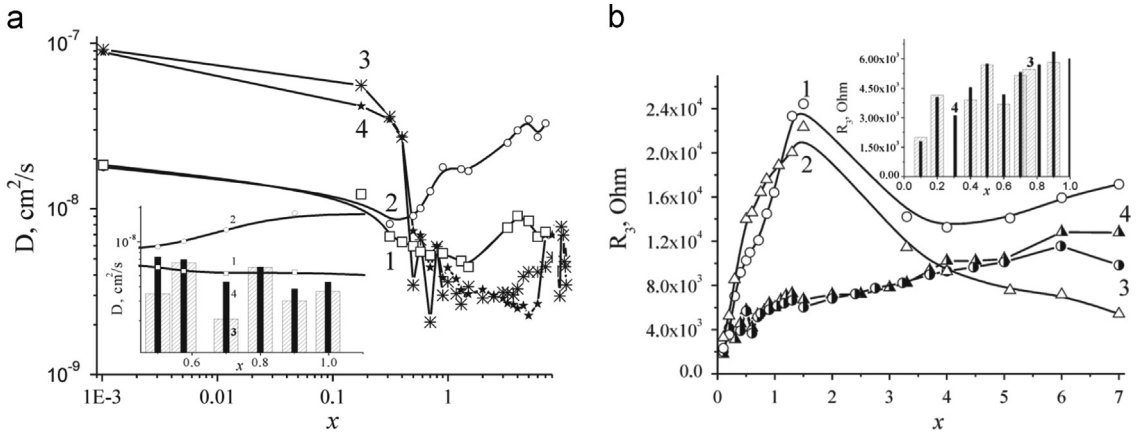

Fig. 3. Diffusion coefficient D (a) and charge transfer resistance R_3 (b) vs guest load degree x in $Mg_3Si_4O_{10}(OH)_2$ fractions: 1 μm (1, 3) and 0.5 μm (2, 4), before (1, 2) and after (3, 4) ultrasonic treatment.

(by 0.07°) shifts the diffraction peak at $2\Theta=33.39°$ to the higher angles. Intensity of the amorphous halo reduces in the range of $11.44\div21.54°$ in both fractions after ultrasonic treatment. The stronger effect of ultrasonic treatment is observed for the structural changes caused by intercalation ($x=7$). Ultrasonic treatment of the 1 μm fraction suppresses diffraction peaks, that appeared at $2\Theta=13.10$ and 16.94° after intercalation and reformats doublet at $2\Theta=33.32°$ into the one peak. In addition, the doublet appears in the vicinity of $2\Theta=17.01°$ only in ultrasonic treated talc after intercalation. Ultrasonic treatment of the 0.5 μm fraction suppresses peak at $2\Theta=22.02°$, shifted after intercalation to $2\Theta=22.78°$, and leads to appearance of the peak at $2\Theta=17.14°$.

Appearance of middle frequency linear areas on Nyquist diagrams, marked by arrows in Fig. 2 (curves 3, 4) is most probably related to ultrasonic effect on the defective subsystem of talc. Such areas are explained by spherical diffusion [8,9], but in our case this interpretation is illegal, because the lamellar form of initial talc has not changed after ultrasonic treatment. That is why appearance of linear areas may be caused by change in type of conductivity from ultimate to complex [7]. Besides it can be explained by visualization of decays of complexes, activated by ultrasonic treatment. In this case the Gerisher impedance [7,10] is used in electric scheme. The reason of linear areas appearance can be caused by common contribution of both described conditions. Then the equivalent electric scheme is presented in the inset b, Fig. 2. In the last case both reactance and electro reactionary behavior are explained by ultrasonic impact on the defect structure of the talc powders.

It is known that the defect concentration, in particular the vacancy concentration in a solid treated with ultrasound depends nonlinearly on both temperature and intensity of acoustic vibration [11,12]. Significant increase of defects in the talc structure is observed in the certain ultrasonic and temperature range. Equilibrium vacancy concentration can be high even at low temperatures [11], while bulk deformation exceeds some critical value. Self-organization of vacancies into separate clusters and periodic structures is possible if their concentration is high enough [13] and they interact one with another and with the crystalline matrix through the deformation field. Formation of the periodic pore lattice in metal and dielectric materials irradiated with high-energy neutron and electron beams is observed in works [14,15].

In works [16–18] it was demonstrated that ultrasonic wave could control the transport properties of semiconductors. Besides it could change their structure due to the processes of impurity atom diffusion, dissolution and formation of complexes impurity atom clusters and intrinsic defects in periodic deformation fields. Moreover the extrinsic heterogeneous deformation causes the change of chemical potential of point defects, thus leading to the directional diffusion flows appearance. In work [19] it was empirically determined that ultrasonic treatment could stimulate Si diffusion at room temperature. Significant increase of carbon diffusion coefficient in steel was observed at fixed temperature in a certain range of acoustic vibration amplitude [20].

In this work, a nonlinear diffusion deformation theory of vacancy cluster formation in a porous material treated with ultrasound is carried out to specify ultrasonic influence on Li^+-intercalation kinetic parameters.

4. Theory

4.1. The model

We model a porous medium by the system of spherical particles (granules). The radius of particles is $r_g=R_0-r_0$, and the radius of impurities is r_d (Fig. 4a), where $2r_0$ is the space between the granules, considered below as the pore diameter (Fig. 4b). We select a cylindrical bulk element of porous material (Fig. 4) with the radius R_0 and the cylindrical pore having the radius r_0 ($R_0 \gg r_0$). The average vacancy concentration of that system is N_{d0}.

Considering the nonlocal Hooke's law [21], the energy of vacancy interaction with matrix atoms U_{da}^{int} through the elastic

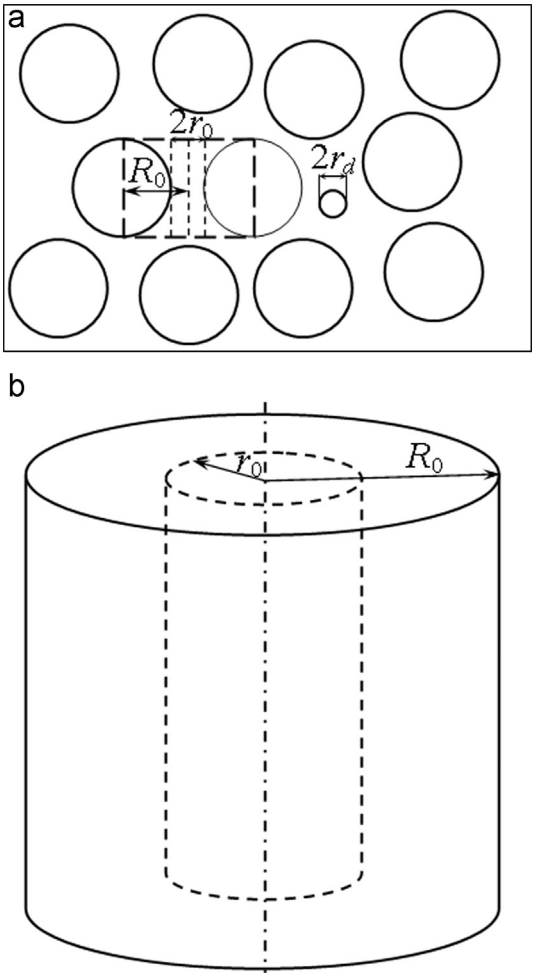

Fig. 4. Geometrical model of a porous medium with impurity.

field can be determined as:

$$U_{da}^{\text{int}}(r) = -\int \lambda(|r'-r|)\varepsilon(r')\Delta\Omega_d\, dr', \tag{1}$$

where λ is the elastic modulus operator [18]. Introducing the variable $\tau = r' - r$ and after Taylor series expansion of $\varepsilon(r+\tau)$ by τ, we obtain:

$$U_{da}^{\text{int}}(r) = -\int \lambda(|\tau|)\varepsilon(r+\tau)\Delta\Omega_d\, d\tau$$

$$= -\int \lambda(\tau)\left(\varepsilon(r) + \frac{\partial^2\varepsilon(r)}{\partial r^2}\frac{\tau^2}{2}\right)\Delta\Omega_d\, d\tau$$

$$= -K\varepsilon(r)\Delta\Omega_d - K\frac{\partial^2\varepsilon(r)}{\partial r^2} r_{da}^2\Delta\Omega_d, \tag{2}$$

where $K = \int\lambda(|\tau|)d\tau$ is an elasticity coefficient [13]; $2r_{da}^2 = (\int\lambda(|\tau|)\tau^2 d\tau / \int\lambda(|\tau|)d\tau)$ is an average value of the squared distance between the vacancy and matrix atoms; $\Delta\Omega_d$ is the change of crystalline volume by one defect; $\varepsilon(r)$ is a radial component of strain tensor.

The elastic field of solid influences the vacancy by force:

$$\vec{F} = -\text{grad}U_{da}^{\text{int}} = K\text{grad}\left(\varepsilon(r)\Delta\Omega_d + \frac{\partial^2\varepsilon(r)}{\partial r^2} r_{da}^2\Delta\Omega_d\right). \tag{3}$$

Under this force, the defects in the elastic field get the velocity

$$\vec{v} = \mu\vec{F} = \frac{D_v K}{k_B T}\text{grad}\left(\varepsilon(r)\Delta\Omega_d + \frac{\partial^2\varepsilon(r)}{\partial r^2} r_{da}^2\Delta\Omega_d\right), \tag{4}$$

where μ, and D_v are the mobility and vacancy diffusion coefficient; T is the temperature; k_B is the Boltzmann constant. Here we use the Einstein relation to determine impurity mobility.

As one can see from Eq. (4), the vacancy rate in the elastic field is determined by deformation gradients and crystal volume gain due to these defects. Thus, the defects that are the compression centers ($\Delta\Omega_d < 0$), in particular vacancies, will move to the area of the relative compression.

Taking Eq. (4) into account, the stationary flow of vacancies can be presented as:

$$j = -D_v\frac{\partial N_d}{\partial r} + N_d\frac{D_v K}{k_B T}\left(\frac{\partial\varepsilon}{\partial r}\Delta\Omega_d + \frac{\partial^3\varepsilon}{\partial r^3} r_{da}^2\Delta\Omega_d\right). \tag{5}$$

Taking into account the anharmonic components, potential energy density of the elastic defects-free continuum can be presented as:

$$U_a = \frac{1}{2}E\varepsilon^2(r) + \frac{1}{3}E\alpha\varepsilon^3(r) + \frac{1}{4}E\beta\varepsilon^4(r) + Ea_0^2\frac{\partial^2\varepsilon(r)}{\partial r^2}\varepsilon(r), \tag{6}$$

where E is the modulus of elasticity; α and β are the elastic enharmonicity constants; a_0 is the characteristic distance of the crystalline matrix atoms interaction that is roughly equal to the matrix lattice parameter.

Then, taking into account Eqs. (2) and (6), free energy density of the crystal with vacancies can be presented as:

$$\Phi = U_a + N_d U_{da}^{\text{int}} - TS$$

$$= \frac{1}{2}E\varepsilon^2(r) + \frac{1}{3}E\alpha\varepsilon^3(r) + \frac{1}{4}E\beta\varepsilon^4(r) + Ea_0^2\frac{\partial^2\varepsilon(r)}{\partial r^2}\varepsilon(r) -$$

$$-KN_d(r)\varepsilon(r)\Delta\Omega_d - KN_d(r)\frac{\partial^2\varepsilon(r)}{\partial r^2} r_{da}^2\Delta\Omega_d - TS, \tag{7}$$

where S is entropy density.

Applying the relation $\sigma = \frac{\partial\Phi}{\partial\varepsilon}$, we obtain the mechanical stress expression:

$$\sigma = E\varepsilon + E\alpha\varepsilon^2 + E\beta\varepsilon^3 + Ea_0^2\frac{\partial^2\varepsilon}{\partial r^2} - KN_d\Delta\Omega_d. \tag{8}$$

The mechanical stress in the ultrasonic treated solid, subject to the enharmonic components, is:

$$\tilde{\sigma} = \sigma + E\varepsilon_0\cos\omega t + E\alpha(\varepsilon_0\cos\omega t)^2 + E\beta(\varepsilon_0\cos\omega t)^3, \tag{9}$$

where ε_0 is deformation amplitude, caused by ultrasound. Here the wave length $\lambda \gg R_0$. Averaging by the time, we obtain:

$$\tilde{\sigma} = E\varepsilon + E\alpha\varepsilon^2\left(1 + \frac{\varepsilon_0^2}{2\varepsilon^2}\right) + E\beta\varepsilon^3 + Ea_0^2\frac{\partial^2\varepsilon}{\partial r^2} - KN_d\Delta\Omega_d =$$

$$E\varepsilon + E\tilde{\alpha}\varepsilon^2 + E\beta\varepsilon^3 + Ea_0^2\frac{\partial^2\varepsilon}{\partial r^2} - KN\Delta\Omega_d, \tag{10}$$

where $\tilde{\alpha} = \alpha\left(1 + \frac{\varepsilon_0^2}{2\varepsilon^2}\right)$.

From the strained solid equilibrium condition $\frac{\partial\tilde{\sigma}}{\partial r}=0$ we obtain the deformation equation:

$$E\frac{\partial\varepsilon}{\partial r}+E\tilde{\alpha}\frac{\partial(\varepsilon^2)}{\partial r}+E\beta\frac{\partial(\varepsilon^3)}{\partial r}+Ea_0^2\frac{\partial^3\varepsilon}{\partial r^3}-K\frac{\partial N_d}{\partial r}\Delta\Omega_d=0. \quad (11)$$

Taking into account Eq. (5), the diffusion steady-state equation for vacancies can be written as:

$$div\left[D_v\frac{\partial N_d}{\partial r}-N_d\frac{D_vK}{k_BT}\left(\frac{\partial\varepsilon}{\partial r}\Delta\Omega_d+\frac{\partial^3\varepsilon}{\partial r^3}r_{da}^2\Delta\Omega_d\right)\right]+G_d-\frac{N_d}{\tau_d}=0, \quad (12)$$

where G_d, and τ_d are the generation rate and vacancy lifetime, respectively.

To find vacancy concentration distribution and deformation in the investigated structure, the system of nonlinear differential Eqs. (11) and (12) should be solved.

Let us present vacancy concentration and deformation as:

$$N_d(r)=N_1(r)+N_0, \quad (13)$$

$$\varepsilon(r)=\varepsilon_1(r)+N_0\Delta\Omega_d, \quad (14)$$

where $N_1(r)$, and $\varepsilon_1(r)$ are the space inhomogeneous components of vacancy concentration and deformation, respectively; $N_1(r)\ll N_0$.

Substituting Eqs. (13) and (14) into Eqs. (11) and (12), and taking into account that $N_1(r)\ll N_0$ and the conditions $(\partial N_1/\partial r)=0$ and $(\partial\varepsilon_1/\partial r)=0$ at $r\to R_0$ must be kept, we obtain that $N_0=G_d\tau_d$ and the equations for $N_1(r)$ and $\varepsilon_1(r)$:

$$D_v\frac{\partial N_1}{\partial r}-N_0\frac{D_v\theta_v}{k_BT}\left(\frac{\partial\varepsilon_1}{\partial r}+\frac{\partial^3\varepsilon_1}{\partial r^3}r_{da}^2\right)=0, \quad (15)$$

$$E\frac{\partial\varepsilon_1}{\partial r}+E\tilde{\alpha}\frac{\partial(\varepsilon_1^2)}{\partial r}+E\beta\frac{\partial(\varepsilon_1^3)}{\partial r}+Ea_0^2\frac{\partial^3\varepsilon_1}{\partial r^3}-\theta_v\frac{\partial N_1}{\partial r}=0, \quad (16)$$

where $\theta_v=K\Delta\Omega_d$ is the vacancy deformation potential.

Integrating Eq. (15), we obtain:

$$N_1=\frac{N_0\theta_v}{k_BT}\left(\varepsilon_1+\frac{\partial^2\varepsilon_1}{\partial r^2}r_{da}^2\right). \quad (17)$$

Substituting Eq. (17) into Eq. (16), we obtain the deformation equation that, after integration, can be written as

$$\frac{\partial^2\varepsilon_1}{\partial r^2}-a\varepsilon_1+f\varepsilon_1^2-c\varepsilon_1^3=0, \quad (18)$$

where

$$a=\frac{1-(N_0/N_c)}{r_{da}^2((N_0/N_c)-(a_0^2/r_{da}^2))};\ f=\frac{|\tilde{\alpha}|}{r_{da}^2((N_0/N_c)-(a_0^2/r_{da}^2))};$$

$$c=\frac{\beta}{r_{da}^2((N_0/N_c)-(a_0^2/r_{da}^2))};\ N_c=\frac{E\cdot k_BT}{\theta_v^2}.$$

Here we have taken into account, that $\alpha<0$, $\beta>0$ [13].

4.2. Formation of vacancy nanoclusters and their periodic structures

The solution of Eq. (18) is

$$r=\int\frac{d\varepsilon_1}{\sqrt{a\varepsilon_1^2-(2f\varepsilon_1^3/3)+(c\varepsilon_1^4/2)}}+r_c,$$

where r_c is the constant of integration.

Replacing $\varepsilon_1=1/z$, one can present this integral as:

$$r-r_c=-\int\frac{dz}{\sqrt{a(z-(f/3a))^2+\Delta}}, \quad (19)$$

where

$$\Delta=-\frac{f^2}{9a}+\frac{c}{2}.$$

The integral (19) is expressed by the analytic functions which type we determine by the sign of the coefficients a and Δ.

If the following conditions are fulfilled:

$$\frac{N_0}{N_c}<\frac{a_0^2}{r_{da}^2}\quad\text{and}\quad\frac{2\tilde{\alpha}^2}{9\beta}<1-\frac{N_0}{N_c}\ (a<0 i\ \Delta<0), \quad (20)$$

then $\varepsilon_1=0$, and $N(r)=N_0$, namely self-organization processes do not take place. Taking into account, that $\frac{2\alpha^2}{9\beta}=\frac{4}{9}$ [13] and

$$\varepsilon^2\approx\frac{\varepsilon_0^2}{2}+\left(\frac{\theta_v}{K}N_0\right)^2,$$

the conditions (20) can be written as

$$\frac{N_0}{N_c}<\frac{a_0^2}{r_{da}^2}\quad\text{and}\quad\varepsilon_0^2<\left(\frac{\sqrt{2}k_BT}{\theta_v}\right)^2\left(\frac{N_0}{N_c}\right)^2\times\left(\frac{1}{(3/2)\sqrt{1-(N_0/N_c)}-1}\right)^{-1}. \quad (21)$$

If average defect concentration exceeds the value of $N_0=N_c(a_0^2/r_{da}^2)$, independently from the ultrasonic wave deformation amplitude, the spatially homogeneous solution becomes unstable, and then a new spatially inhomogeneous stationary state (formation of clusters or periodic vacancy structures) appears. Besides, if the 2nd condition in (21) is not fulfilled, vacancy clusters will always appear. If concentration of clusters or periodic vacancy structures is constant, then their formation conditions depend on the temperature. In particular, the conditions (21) can be written as:

$$\frac{T_c}{T}<\frac{a_0^2}{r_{da}^2},\ \varepsilon_0^2<\left(\frac{\sqrt{2}k_BT_c}{\theta_v}\right)^2\left(\frac{1}{(3/2)\sqrt{1-(T_c/T)}-1}\right)^{-1}, \quad (22)$$

where

$$T_c=\frac{\theta_v^2N_0}{E\cdot k_B}.$$

In other cases, depending on the values N_0 (T) and ε_0, the solution of Eq. (18) will be:

$a>0$ and $\Delta>0$:

$$\varepsilon_1(r)=-\frac{A}{B+sh(-\sqrt{a}(r-r_0))} \quad \text{at} \quad \frac{a_0^2}{r_{da}^2}<\frac{N_0}{N_c}<1-\frac{2\tilde{\alpha}^2}{9\beta}. \quad \text{and}$$

$$\varepsilon_0^2<\left(\frac{\sqrt{2}k_БT}{\theta_v}\right)^2\left(\frac{N_0}{N_c}\right)^2\left(\frac{1}{(3/2)\sqrt{1-(N_0/N_c)}-1}-1\right)^{-1}; \tag{23}$$

$a>0$ and $\Delta<0$:

$$\varepsilon_1(r)=-\frac{A}{B+ch(\sqrt{a}(r-r_0))} \quad \text{at} \quad 1-\frac{2\tilde{\alpha}^2}{9\beta}<\frac{N_0}{N_c}<1$$

and

$$\varepsilon_0^2<\left(\frac{\sqrt{2}k_БT}{\theta_v}\right)^2\left(\frac{N_0}{N_c}\right)^2\left(\frac{1}{\frac{3}{2}\sqrt{1-(N_0/N_c)}-1}-1\right)^{-1},,$$

or at

$$\frac{a_0^2}{r_{da}^2}<\frac{N_0}{N_c}<1-\frac{2\tilde{\alpha}^2}{9\beta},\ \varepsilon_0^2>\left(\frac{\sqrt{2}k_БT}{\theta_v}\right)^2\left(\frac{N_0}{N_c}\right)^2\times\left(\frac{1}{(3/2)\sqrt{1-(N_0/N_c)}-1}-1\right)^{-1} \tag{24}$$

$a<0$ and $\Delta>0$:

$$\varepsilon_1(r)=-\frac{A}{B+\ \sin(\sqrt{|a|}(r-r_0))} \quad \text{at} \quad \frac{N_0}{N_c}>1 \quad \text{and}$$

$$\varepsilon_0^2<\left(\frac{\sqrt{2}k_БT}{\theta_v}\right)^2\left(\frac{N_0}{N_c}\right)^2\left(\frac{1}{(3/2)\sqrt{1-(N_0/N_c)}-1}-1\right)^{-1},$$

or at

$$\varepsilon_0^2>\left(\frac{\sqrt{2}k_БT}{\theta_v}\right)^2\left(\frac{N_0}{N_c}\right)^2\left(\frac{1}{\frac{3}{2}\sqrt{1-\frac{N_0}{N_c}}-1}-1\right)^{-1}$$

$$\text{and} \quad \frac{N_0}{N_c}<\frac{a_0^2}{r_{da}^2} \tag{25}$$

where

$$A=3\sqrt{2}|a|(|9ca-2f^2|)^{-1/2};B=\sqrt{2}f(9ca-2f^2)^{-1/2}.$$

The constant of integration r_c is chosen because the maximum vacancy clustering occurs at the pore surface, so that the condition $r_c=r_0$ is fulfilled.

Thus, vacancy clusters or their periodic structures are formed at certain values of the defect concentration N_0 (or the temperature T) and ultrasonic wave amplitude ε_0. In Fig. 5 the areas of possible formation of vacancy clusters depending on the values ε_0^2 and (N_0/N_c) (T_c/T) are plotted. Calculations are carried out for the following parameter values: $(a_0^2/r_{da}^2)=0.01$; $(\sqrt{2}k_БT/\theta_v)=0.01$.

Substituting the formulas (23)–(25) into (17), we can find the vacancy concentration. Fig. 6 shows the spatial vacancy concentration distribution (when a symmetric cluster is formed) in the vicinity of a pore with the radius r_0.

The cluster radius depends on the defect concentration, elastic constants, and temperature, and can be determined as:

$$r_{cluster}=\frac{1}{\sqrt{a}}=r_{da}\sqrt{\frac{(N_0/N_c)-(a_0^2/r_{da}^2)}{1-(N_0/N_c)}} \tag{26}$$

or

$$r_{cluster}=\frac{1}{\sqrt{a}}=r_{da}\sqrt{\frac{(T_c/T)-(a_0^2/r_{da}^2)}{1-(T_c/T)}}. \tag{27}$$

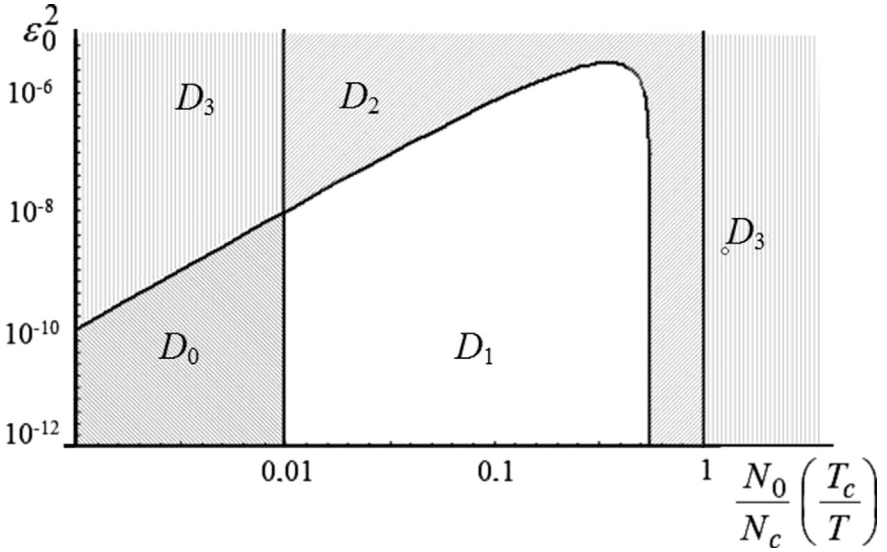

Fig. 5. Areas of possible vacancy cluster formation depending on the values of ε_0^2 and (N_0/N_c) (T_c/T): D_0 is the no vacancy self-organization processes occur; D_1 is the region, where the asymmetric vacancy cluster appears (Eq. (23)); D_2 is the region, where the symmetric vacancy cluster appears (Eq. (24)); D_3 is the region, where the periodic vacancy lattice appears (Eq. (25)).

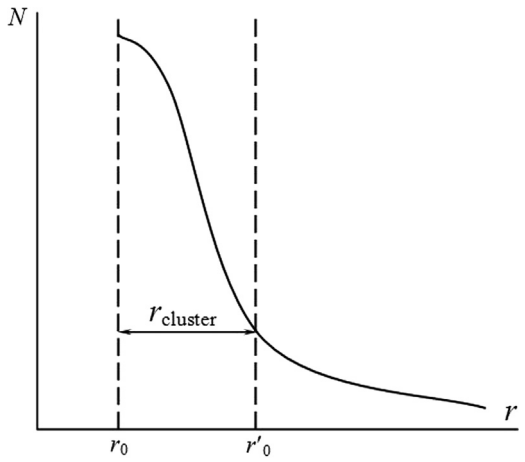

Fig. 6. Spatial vacancy concentration distribution in the vicinity of the pore.

The cluster radius has nano-range value and increases monotonically with vacancy concentration increase (temperature decrease).

4.3. Diffusion coefficient

Vacancy clusters or their periodic structures are formed, when the vacancy concentration exceeds a certain critical value (at the temperature lower, than a certain critical value). Then it can be considered, that the porosity of the structure will increase due to the pore expansion and formation of new ones. The pore size r_0' at the surface of which a vacancy cluster is formed can be determined in the following way (Fig. 6):

$$r_0^{'} = r_0 + r_{cluster}. \tag{28}$$

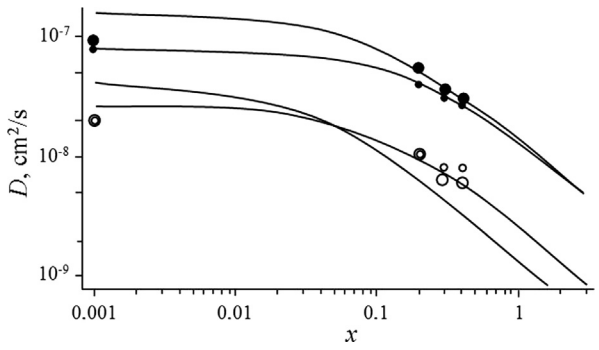

Fig. 7. Dependence of the diffusion coefficient of Li impurities in $Mg_3Si_4O_{10}(OH)_2$ structure on their relative concentration x: $2R_0=1$ μm (curves 1, 3) and $2R_0=0.5$ μm (curves 2, 4); before (curves 1, 2) and after (curves 3, 4) the ultrasonic treatment; ●● – experimental points after the ultrasonic treatment at $2R_0=1$ μm and $2R_0=0.5$ μm, respectively; ○○ – experimental points before the ultrasonic treatment at $2R_0=1$ μm and $2R_0=0.5$ μm, respectively.

are moving as well and the granules are motionless, the full number of the collisions can be presented as:

$$z = 4\sqrt{2}\pi r_d^2 n_0 \overline{\upsilon} + \pi(r_d + R_0 - r_0)^2 n_g \overline{\upsilon}, \tag{30}$$

where n_g, and n_0 are the granule and impurities concentration in the granule-free bulk.

The impurity concentration in the granule-free bulk can be calculated through the molecule concentration in the full bulk of the structure n as $n_0 = n(R_0^3/R_0^3 - (R_0 - r_0)^3)$. Then the diffusion coefficient can be written as:

$$D_0 = \frac{\overline{\upsilon}}{3\left(4\sqrt{2}\pi r_d^2 n(R_0^3/R_0^3 - (R_0 - r_0)^3) + \frac{3}{4R_0^3}(r_d + R_0 - r_0)^2\right)}. \tag{31}$$

Taking into account Eq. (28), we obtain the diffusion coefficient vs the vacancy cluster size:

$$D_{0US} = \frac{\overline{\upsilon}}{3(4\sqrt{2}\pi r_d^2 n(R_0^3/R_0^3 - (R_0 - r_0 - r_{cluster})^3) + (3/4R_0^3)(r_d + R_0 - r_0 - r_{cluster})^2)}. \tag{32}$$

Let us find the dependence of the impurities diffusion coefficient D of the porous structure dependently from pores' radius, within the kinetic theory.

Diffusion coefficient of gases:

$$D_0 = \frac{\overline{\upsilon}^2}{3z}, \tag{29}$$

where $\overline{\upsilon}$ is the arithmetic average velocity of impurities; z is the number of collisions of impurity with other impurities and granules of porous structure per unit of time.

We define the number of collisions of impurity with other impurities and granules of porous structure as the sum separately of the collisions with impurities and the collisions with granules. For this purpose we consider that the impurities and the granules are the spheres with the radii r_d and $(R_0 - r_0)$, respectively (Fig. 4). Taking into account, that other impurities

Fig. 7 shows the theoretical calculation results and the empirical data of the dependence of the diffusion coefficient D of Li^+ impurities in $Mg_3Si_4O_{10}(OH)_2$ structure vs relative concentration of x. Calculations are carried out under the following conditions: $r_0=5$ nm, $r_0=5$ nm, $(N_0/N_c)=0.8$, $r_d=0.106$ nm, $a_0=0.5$ nm.

The increase of Li^+ diffusion coefficient in ultrasonically treated talc corresponds to the calculation results within the proposed model. The theoretical results agree well with the empirical results at low impurity concentrations, as far as we have applied the kinetic theory of gases to calculate the diffusion coefficient. Besides, inhomogeneous deformation fields, appearing in the vicinity of self-organized defect clusters can retract or, contrary, eject the diffusing impurities depending on the type of deformation gradient and the kind of deformation generated by the impurity.

5. Conclusion

1. Ultrasonic treatment of talc natural mineral in 1 M $LiBF_4$ in γ-butyrolactone solution during 8 h at the frequency of 22 kHz is an effective modification method to increase power capacity even at a sufficiently deep discharge level ($x \approx 4$).
2. The aftereffect of ultrasonic treatment on the talc structure and Gibbs' energy of Li^+-intercalation current formation process depends on the particle size. The phase diagram of the intercalated phase has completely changed after ultrasonic treatment.
3. Ultrasonic treatment of talc causes oscillations of diffusion coefficient $D(x)$ and stage charge transfer resistance $R_3(x)$ with x, which is the result of changes in electronic energy topology caused by ultrasonic effect on a defective subsystem.
4. Formation of vacancy nanoclusters and their periodic structures in a porous material, treated with ultrasound, is the base of the nonlinear diffusion deformation model. This model foresees significant diffusion coefficient increase. This result coincides with the experimental one.

References

[1] N.F. Solodkii, A.S. Shamrikov, V.M. Pogrebenkov, The Ural mineral raw-material base for the ceramics, refractory, and glass industry. Reference manual under the editorship Professor G.N. Maslennikova, TNU, Tomsk, 2009.
[2] I.I. Grygorchak, Talc as a new host material in intercalation nanotechnologies, Rep. NAS Ukr. 6 (2002) 110–113.
[3] A. Pidluzhna, I. Grigorchak, M. Nikipanchuk, B. Ostafiychuk, I. Budzulyak, M. Mitsov, L. Yablon, Intercalation current generation in oxygen- and sulfur-doped talc, Rus. J. Electrochem. 48 (2012) 545–549.
[4] L.A. Perez-Maqueda, A. Duran, J.L. Perez-Rodriguez, Preparation of submicron talc particles by sonication, Appl. Clay Sci. 5 (2005) 145–255.
[5] E.M. Zobov, M.E. Zobov, F.S. Gabibov, I.K. Kamilov, F.I. Manyakhin, E.K. Naimi, Effect of ultrasonic treatment on photoelectric and luminescent properties of ZnSe crystals, Semiconductors 42 (2008) 277–280.
[6] P.B. Parchinsky, S. Vlasov, R.A. Muminov, et al., The effect of ultrasound on the parameters of metal-insulator-semiconductor, Tech. Phys. Lett. 26 (2000) 40–45.
[7] Z.B. Stoynov, B.M. Grafov, B.S. Savova-Stoynova, V.V. Yolkin, in: Electrochemical Impedance, Nauka, Moscow, 1991.
[8] M.D. Levi, D. Aurbach, Impedance of a single intercalation particle and of non-homogeneous, multilayered porous composite electrodes for Li-ion batteries, J. Phys. Chem. 108 (2004) 11693–11703.
[9] Martin Z. Bazant Juhyun Songa, Effects of nanoparticle geometry and size distribution on diffusion impedance of battery electrodes, J. Electrochem. Soc. 160 (2013) A15–A24.
[10] N.A. Sekushin, Properties of Warburg and Gerischer diffusion impedances in low frequencies region, News of the Komi Scientific Center, RAS 4 (2010) 22–27.
[11] L.A. Bulavin, O.Yu. Aktan, Yu.F. Zabashta, Vacancies in a strongly strained crystal at low temperatures, Phys. Solid State 50 (2008) 2270–2274.
[12] O.V. Abramov, Ultrasound in Liquid and Solid Metals, Russian Academy of Sciences, Moscow, 1993 (in English).
[13] V.I. Emel'yanov, I.M. Panin, Formation of nanometer ordered defect-deformational structures induced by energy fluxes in solids, Fiz. Tverd. Tela 39 (1997) 2029–2035 (in Rus.).
[14] V.K. Sikka, J. Moteff, Damage in neutron-irradiated molybdenum (I). Characterization of as-irradiated microstructure, J. Nucl. Mater. 54 (1974) 325–345.
[15] L.T. Chadderton, E. Johnson, T. Wohlenberg, Observations of a regular void array in natural fluorite irradiated with 100 keV electrons, Phys. Scr. 13 (1976) 127–128.
[16] B.H. Zaveryuhin, H.H. Zaveryuhina, O.M. Tursunkulov, Changes in the reflection coefficient of the radiation from the semiconductor surface in the spectral range $\lambda = 0.2$-20 μm under the influence of ultrasonic waves, Techn. Phys. Lett. 28 (2002) l–12.
[17] O.Ya. Olikh, I.V. Ostrovskii, Ultrasound-stimulated increase in the electron diffusion length in p-Si crystals, Phys. Solid State 44 (2002) 1249–1253.
[18] S. Ostapenko, R. Bell, Ultrasound stimulated dissociation of Fe-B pairs in silicon, J. Appl. Phys. 77 (1995) 5458–5460.
[19] I.V. Ostrovskii, A.B. Nadtochii, A.A. Podolyan, Ultrasonically stimulated low-temperature redistribution of impurities in silicon, Semiconductors 36 (2002) 367–369.
[20] A.V. Kulemin, Ultrasound and Diffusion in Metals, Metallurgiya, Moscow, 1978 (in Rus.).
[21] I.A. Kunin, Nonlocal Theory of Elasticity, Polish Academy of Sciences, Warsaw, 1970.